



The Twin-Well Duffing Equation: Escape Phenomena, Bistability, Jumps, and Other Bifurcations

J. Kyzioł and A. Okniński *

Politechnika Świętokrzyska, Al. 1000-lecia PP 7, 25-314 Kielce, Poland.

Received: August 3, 2023; Revised: February 24, 2024

Abstract: In this work, we investigate the escape phenomenon, the onset of bistability, jumps, as well as other bifurcations present in the twin-well Duffing equation. Based on the known steady-state asymptotic solution – the amplitude-frequency implicit function – and using the theory of differential properties of implicit functions, we compute the singular and critical points of this function. This enables us to predict several bifurcations present in the dynamical system under study. The main result is the calculation of the escape bifurcation set – the set of parameters for which escape phenomena occur, and equations to compute the onset of bistability.

Keywords: *metamorphoses of amplitude-frequency curves; bifurcations.*

Mathematics Subject Classification (2010): 34C05, 34C25, 34E05, 37G35, 70K20, 70K30, 70K50.

1 Introduction and Motivation

We study the dynamics of a vibrating system governed by the Duffing equation with negative linear stiffness [1, 2]:

$$\frac{d^2x}{dt^2} + k \frac{dx}{dt} - \alpha x + \gamma x^3 = f \cos \omega t \quad (k, \alpha, \gamma > 0). \quad (1)$$

After rescaling the variables as in [2]:

$$\tau = t\sqrt{\alpha}, \quad y = \alpha x, \quad h = k/\sqrt{\alpha} > 0, \quad c = \gamma/\alpha^3 > 0, \quad \Omega = \omega/\sqrt{\alpha}, \quad (2)$$

we obtain the nondimensional Duffing equation

* Corresponding author: <mailto:fizao@tu.kielce.pl>

$$\frac{d^2y}{d\tau^2} + h \frac{dy}{d\tau} - y + cy^3 = f \cos \Omega\tau \quad (h, c > 0), \quad (3)$$

which is a twin-well potential system with a potential function $V(y) = \frac{1}{2}y^2 - \frac{1}{4}cy^4 + C$ (note that for $h = 2\zeta$, $c = \gamma$, we get equation (7.1.2) of [2]). Equation (3) appears in many physical problems, in early applications, it was used to model buckled beam dynamics [3, 4], see also [5] and references therein.

Many bifurcations of dynamics occurring in equation (3) were described before [1, 2]. The motivation of this work is to find and classify all bifurcations of the dynamics by studying qualitative changes in the differential properties of the approximate asymptotic solution (metamorphoses) of the Duffing equation (3).

Our main aim is to investigate an escape phenomenon, i.e., a transition from one well to cross-well motion under a smooth transition of a control parameter. This is an important problem since such a transition can result in a sudden increase in the amplitude of vibration with serious consequences for a vibrating construction. Moreover, we also aim at determining the onset of bistability and emergence of jump phenomena.

In the next section, we describe the methods used to find approximate asymptotic solutions of Eq.(3) and to study their differential properties. The equations for singular points and vertical tangencies are solved in Sections 3 and 4, respectively. In Section 5, we verify our analytical calculations by solving Eq.(3) numerically and summarize our results in the last section.

2 Methods

Our approach is based on: (i) the asymptotic solutions of nonlinear differential equations and (ii) the differential properties of implicit functions, see [6] and references therein. The idea to use the Implicit Function Theorem to "define and find different branches intersecting at the singular points of amplitude profiles" was proposed in [7].

Let us now look how the 1 : 1 resonance can be computed within the asymptotic approach [8–10]. For small nonzero ε , the asymptotic solutions of Eq.(3) are assumed in the form

$$y(\tau) = A_0 + A \cos(\Omega\tau + \varphi) + \varepsilon y_1(A_0, A, \varphi, \tau) + \dots \quad (4)$$

Working in the spirit of [10], Section 13.5, we get the following conditions for the steady-states:

$$K_1(A_0, A) = A_0 \left(\frac{3}{2}A^2c + cA_0^2 - 1 \right) = 0, \quad (5a)$$

$$K_2(A_0, A, \Omega) = h^2A^2\Omega^2 + A^2 \left(\Omega^2 + 1 - 3cA_0^2 - \frac{3}{4}cA^2 \right)^2 - f^2 = 0. \quad (5b)$$

Furthermore, following [10] again, we can solve Eq.(5a) for A_0 and substitute to (5b) obtaining the Type I (small orbits) solutions

$$L_1(A, \Omega) = h^2A^2\Omega^2 + A^2 \left(\Omega^2 - 2 + \frac{15}{4}cA^2 \right)^2 - f^2 = 0 \quad (cA_0^2 = 1 - \frac{3}{2}A^2c > 0), \quad (6)$$

and the Type II (large orbits) ones

$$L_2(A, \Omega) = h^2A^2\Omega^2 + A^2 \left(\Omega^2 + 1 - \frac{3}{4}cA^2 \right)^2 - f^2 = 0 \quad (A_0 = 0). \quad (7)$$

We now start our analysis of the differential properties of implicit functions K_1 , K_2 , see Eqs.(5). Equations (5) describe a curve in the three-dimensional (3D) space (A_0, A, Ω) , being an intersection of two surfaces, $K_1(A_0, A) = 0$ and $K_2(A_0, A, \Omega) = 0$.

The singular points of this curve are computed from the following equations [11, 12]:

$$\left. \begin{aligned} & K_1(A_0, A) = 0 \\ & K_2(A_0, A, \Omega) = 0 \\ & \det \begin{pmatrix} \frac{\partial K_1}{\partial A_0} & \frac{\partial K_2}{\partial A_0} \\ \frac{\partial K_1}{\partial A} & \frac{\partial K_2}{\partial A} \end{pmatrix} = 0 \\ & \det \begin{pmatrix} \frac{\partial K_1}{\partial A_0} & \frac{\partial K_2}{\partial A_0} \\ \frac{\partial K_1}{\partial \Omega} & \frac{\partial K_2}{\partial \Omega} \end{pmatrix} = 0 \\ & \det \begin{pmatrix} \frac{\partial K_1}{\partial A} & \frac{\partial K_2}{\partial A} \\ \frac{\partial K_1}{\partial \Omega} & \frac{\partial K_2}{\partial \Omega} \end{pmatrix} = 0 \end{aligned} \right\}. \tag{8}$$

The determinant conditions in (8) mean that at a singular point, the continuous and differentiable functions $A_0(\Omega)$, $A(\Omega)$, and $A_0(A)$, $\Omega(A)$, as well as $A(A_0)$, $\Omega(A_0)$ do not exist.

In the neighborhood of a singular point $(A_{0*}, A_*, \Omega_*; h_*, c_*, f_*)$, the 3D curve, defined by Eqs.(5), changes its form. Accordingly, the bifurcation diagram changes its form as well, i.e., the dynamics undergoes a bifurcation.

Alternatively, we analyze simpler 2D curves defined in Eqs.(6), (7). The conditions for singular points are [11, 13]

$$\left. \begin{aligned} & L_i(A, \Omega; h, c, f) = 0 \\ & \frac{\partial L_i(A, \Omega; h, c, f)}{\partial \Omega} = 0 \\ & \frac{\partial L_i(A, \Omega; h, c, f)}{\partial A} = 0 \end{aligned} \right\}, \tag{9}$$

where $i = 1, 2$ and the functions L_1, L_2 are defined in Eqs.(6), (7), respectively.

The second and third conditions in (9) entail that at a singular point, the continuous and differentiable functions $\Omega(A)$ or $A(\Omega)$ do not exist. Accordingly, the amplitude response curve $L_i(A, \Omega; h, c, f) = 0$ changes its differential properties at a singular point $(\Omega_*, A_*; h_*, c_*, f_*)$.

The metamorphoses of the amplitude-frequency curves (i.e., the changes of differential properties) can also occur in a non-singular setting. More precisely, a metamorphosis of this kind occurs when a smooth change of parameters leads to the formation of vertical tangential points of an amplitude [14–16]. It follows that the equations guaranteeing the formation of a (non-singular) vertical tangential point (A_*, Ω_*) are

$$\left. \begin{aligned} & L_i(A, \Omega; h, c, f) = 0 \\ & \frac{\partial L_i(A, \Omega; h, c, f)}{\partial A} = 0 \end{aligned} \right\} \quad (i = 1, 2). \tag{10}$$

More precisely, the second of conditions (10) entails that the function $A(\Omega)$ has a vertical tangency (the continuous and differentiable function $A(\Omega)$ does not exist).

Finally, the equations

$$\left. \begin{aligned} & L_i(A, \Omega; h, c, f) = 0 \\ & \frac{\partial L_i(A, \Omega; h, c, f)}{\partial \Omega} = 0 \end{aligned} \right\} \quad (i = 1, 2), \tag{11}$$

are conditions for the maxima, minima, and inflection points of the function $A(\Omega)$ [11] (the function $\Omega(A)$ has a vertical tangency at any of these points).

Equations (8), (9), (10), (11) are general and permit the prediction of the diverse metamorphoses of amplitude-frequency response implicit functions, see [17] in the context of Eqs.(8) and [6] and references therein for a review of the applications of Eqs.(9), (10).

However, in simple cases such as the Duffing equation, the metamorphoses of amplitude profiles, induced by a change of parameters, were predicted without invoking the differential theory of implicit curves in pioneering papers [14–16, 18].

For example, jumps were computed algebraically in [14] (in the framework of Catastrophe Theory) and in [19]. Moreover, a differential condition for jumps was obtained in [15, 16]. Furthermore, the merging of two parts of the amplitude-frequency response curve, equivalent to a singularity, was computed in [18] (see also [16] and references therein).

While the changes in the differential properties of asymptotic solutions are important, the stability of the solutions is another essential factor shaping the dynamics.

3 Singular Points

A solution of Eqs.(8) is a curve in the 3D space of state variables A_0 , A , Ω , with the parameters h , c , f . Therefore, we shall look for the singular points of this curve in the most general 3D setting. The physical solutions of Eqs.(8) are shown in Table 1,

Type I (small orbits)	Type II (large orbits)
$A_0 = \frac{\sqrt{15c}}{15c} \sqrt{11 - 2\Omega^2}$	$A_0 = 0$
$A = \frac{2\sqrt{5c}}{15c} \sqrt{\Omega^2 + 2} \leq \sqrt{\frac{2}{3c}}$	$A = \sqrt{\frac{2}{3c}}$
$h = \frac{2\sqrt{6}}{3} \sqrt{1 - \Omega^2}$	h – arbitrary
$f = \frac{4(\Omega^2+2)\sqrt{10c}}{45c} \sqrt{1 - \Omega^2}$	$f = \frac{\sqrt{6c}}{6c} \sqrt{4\Omega^4 + 4(h^2 + 1)\Omega^2 + 1}$
$c > 0$	$c > 0$
$ \Omega \leq 1$	Ω – arbitrary

Table 1: Singular points: physical solutions of Eqs.(8).

where inequality (7) was used in the second row of the first column. There are also other, borderline physical solutions of Eqs.(8) with $h = f = 0$, see Table 2.

Type I (small orbits)	Type II (large orbits)
$A_0 \neq 0$	$A_0 = 0$
$A = 2A_0 \sqrt{\frac{2-\Omega^2}{6\Omega^2+3}}$	$A = 2\sqrt{\frac{\Omega^2+1}{3c}}$
$h = 0$	$h = 0$
$f = 0$	$f = 0$
$c = \frac{2\Omega^2+1}{5A_0^2}$	$c \neq 0$
$ \Omega \leq \sqrt{2}$	Ω – arbitrary

Table 2: Borderline physical solutions of Eqs.(8).

Alternatively, we look for singular points in a simpler, less general 2D formulation (9).

It turns out that there are physical singular points of the 2D implicit curve $L_1(A, \Omega; h, c, f) = 0$, equivalent to the solution in the first column shown in Table 1. On the other hand, the implicit curve $L_2(A, \Omega; h, c, f) = 0$ has no physical singular points. There are, however, borderline singular points listed in Table 2, see Section 5.

It follows that the solutions displayed in the second column of Table 1 can be obtained in the 3D formulation only. These solutions describe, as we shall show below, a transition between small and large orbits. The bifurcation set, the set of parameters, for a given value of Ω , for which there is a Type II solution displayed in Table 1,

$$4\Omega^4 + 4(h^2 + 1)\Omega^2 + 1 = 6cf^2, \tag{12}$$

cf. the 4th row of the Table, is shown in Fig.1.

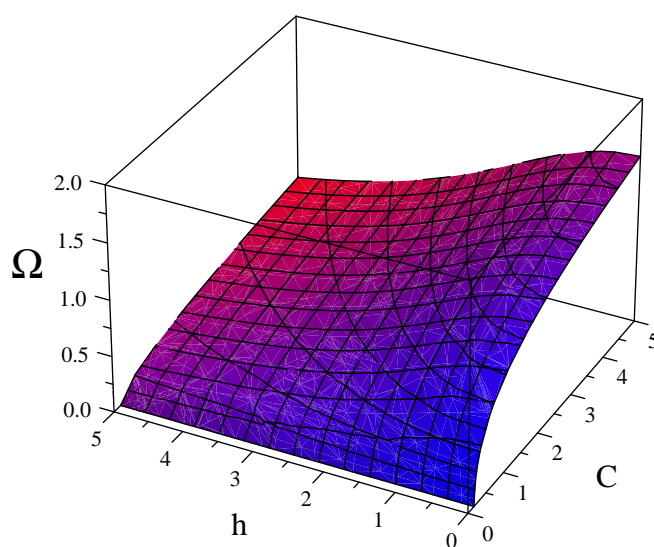


Figure 1: The bifurcation set, $4\Omega^4 + 4(h^2 + 1)\Omega^2 + 1 = 6C$, $C = cf^2$.

4 Jumps, Singular Points, and the Onset of Bistability

The jump equations (10) can be simplified. More precisely, we compute from (10) the equation for the amplitude A only,

$$\left. \begin{aligned} &\beta_5^{(i)} c^3 h^2 Z^5 + \beta_4^{(i)} c^2 h^2 Z^4 + \beta_3^{(i)} c^2 f^2 Z^3 + \beta_2^{(i)} ch^2 f^2 Z^2 + 16f^4 = 0, \\ &\beta_5^{(1)} = -3375, \quad \beta_4^{(1)} = 1800, \quad \beta_3^{(1)} = -900, \quad \beta_2^{(1)} = -120, \\ &\beta_5^{(2)} = 27, \quad \beta_4^{(2)} = -36, \quad \beta_3^{(2)} = -36, \quad \beta_2^{(2)} = 24, \end{aligned} \right\} \tag{13}$$

$Z = A^2$, and, after a value of A is calculated, an equation for the frequency Ω is obtained:

$$\left. \begin{aligned} &\gamma_6^{(i)} c^2 h^2 Z^3 + \gamma_4^{(i)} ch^2 Z^2 + \gamma_2^{(i)} cf^2 Z + 8\gamma_0^{(i)} f^2 + 8f^2\Omega^2 = 0, \\ &\gamma_3^{(1)} = 225, \quad \gamma_2^{(1)} = -120, \quad \gamma_1^{(1)} = 90, \quad \gamma_0^{(1)} = h^2 - 2, \\ &\gamma_3^{(2)} = 9, \quad \gamma_2^{(2)} = -12, \quad \gamma_1^{(2)} = -18, \quad \gamma_0^{(2)} = h^2 + 1, \end{aligned} \right\} \tag{14}$$

where $i = 1$ means that we solve Eqs.(10) for the function L_1 , while $i = 2$ means that we solve Eqs.(10) for the function L_2 , with the functions L_1, L_2 defined in equations (6) and (7), respectively.

The physical ($A > 0, \Omega > 0$) single roots of Eqs.(10) describe jumps. We now consider an important case of the double (multiple) roots of (10).

The multiple roots of Eqs.(13) occur at the parameter values for which the discriminants D_i of polynomials in Eqs.(13) vanish. The discriminant of a polynomial can be computed as a determinant of the corresponding 9×9 Sylvester matrix, see [20] and Eq.(13) in [6]. In the case of small orbits ($i = 1$), we have

$$D_1(h, c, f) = p_1(h, c, f) q_1(h, c, f) = 0, \quad (15a)$$

$$p_1(h, c, f) = h^6 - 16h^4 + 64h^2 - 240f^2c, \quad (15b)$$

$$q_1(h, c, f) = (12960f^2c - 8192)h^6 + 25920cf^2h^4 + 6075c^2f^4. \quad (15c)$$

The singular points of small orbits are given by the equation $p_1(h, c, f) = 0$, which has the physical solutions listed in the first column of Table 1. The onset of bistability, corresponding to a double root of Eq.(13), is given by the equation $q_1(h, c, f) = 0$.

In the case of large orbits ($i = 2$), the determinant is

$$D_2(h, c, f) = p_2(h, c, f) q_2(h, c, f) = 0, \quad (16a)$$

$$p_2(h, c, f) = h^6 + 8h^4 + 16h^2 + 48f^2c, \quad (16b)$$

$$q_2(h, c, f) = (1024 - 2592f^2c)h^6 + 2592cf^2h^4 + 243c^2f^4. \quad (16c)$$

The singular points of the large orbit are given by the equation $p_2(h, c, f) = 0$, which has no real solutions for $c > 0$. Therefore, a large orbit has the singular points listed in the second column of Table 1 only. Furthermore, the equation $q_2(h, c, f) = 0$ determines the onset of bistability.

5 Numerical Verification and Analysis of the Analytical Results

5.1 Small orbits: singular points and the onset of bistability

The formulas for the Type I singular points are listed in the first column of Table 1. We choose $c = 1, \Omega = 0.8$. Then the equations listed in the first column of Table 1 yield $h = 0.979796, f = 0.445249$, and $A_0 = 0.804984, A = 0.484424$.

Now, we plot the implicit function $L_1(A, \Omega) = 0$, defined in Eq.(6), for $h = 0.979796, c = 1$, and three values of f : $f = 0.44$ (green), $f = 0.445249$ (red, analytical critical), $f = 0.46$ (blue), see Fig.2. The amplitude-frequency curve has a singular point – an intersection. Therefore, we can expect a rupture of a stable branch of solution (4), corresponding to the green line in Fig.2.

The corresponding bifurcation diagrams, computed from Eq.(3) for $h = 0.979796, c = 1$, and two values of f : $f = 0.59900$ (below the numerical critical value), $f = 0.59914$ (above the numerical critical value), are shown in Fig.3. Blue and green colors in Figure 3 correspond to blue and green branches in Fig.2.

Indeed, it follows that the upper blue branch in Fig.2 is continuous, see the upper blue curve in Fig.3. On the other hand, after the metamorphosis, see the red curve, the upper green curve in Fig.3 must be ruptured since the green branches in Fig.2 are disconnected. Note that, while the gap in the green branch in Fig.3 occurs near the critical value

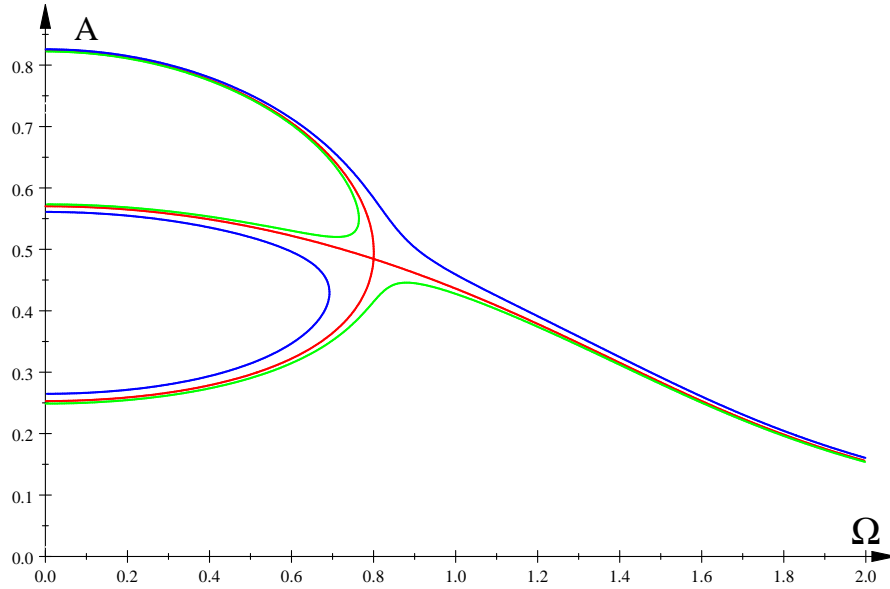


Figure 2: Implicit functions $L_1(A, \Omega; h, c, f) = 0$: $h = 0.979796$, $c = 1$, $f = 0.44$ (green), $f = 0.445249$ (red), $f = 0.46$ (blue).

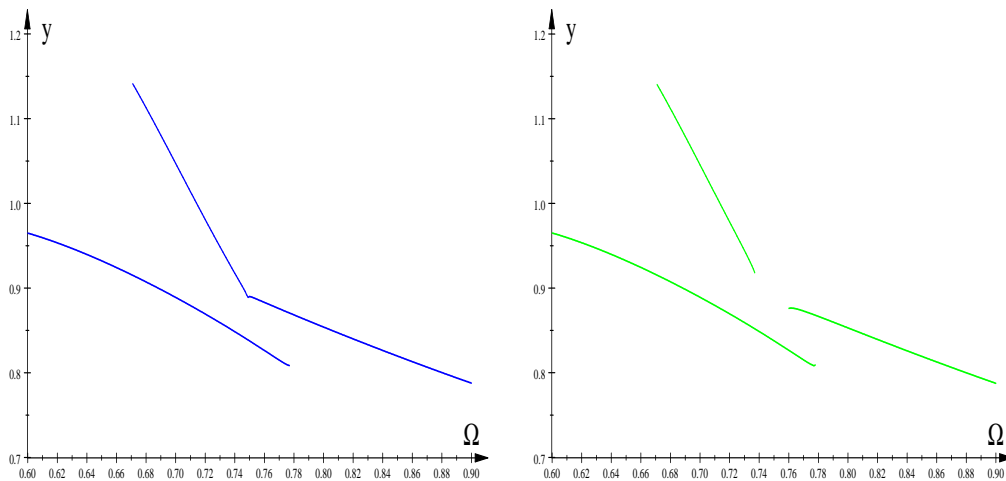


Figure 3: Bifurcation diagrams $y(\Omega)$ for Eq.(3): $h = 0.979796$, $c = 1$, $f = 0.59914$ (blue), and $f = 0.59900$ (green).

$\Omega = 0.8$, the numerical critical value of the parameter f , $f \in (0.59900, 0.59914)$, is quite far from the analytical value $f = 0.445249$.

We now use equations (15) from Section 4 to study jump phenomena. Let $h = 0.1$, $c = 1$. Then the equation $p_1(h, c, f) = 0$ yields the real solution $f = 0.051575$, corresponding to a singular point. On the other hand, the equation $q_1(h, c, f) = 0$ has the real solution $f = 0.031088$ which determines the onset of bista-

bility. In the left Figure 4, the amplitude-frequency curves are shown and the right Figure 4 shows the bifurcation diagram computed for Eq.(3).

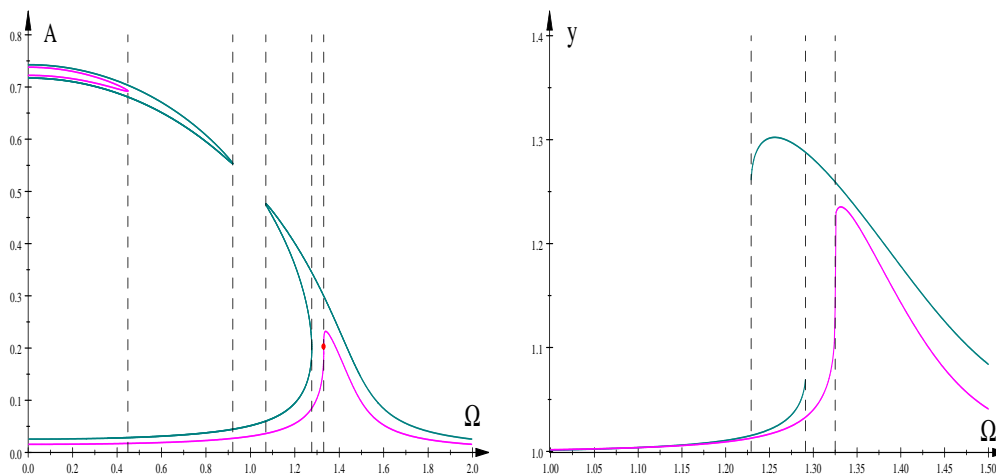


Figure 4: Functions $L_1(A, \Omega) = 0$: $h = 0.1$, $c = 1$, $f = 0.031\ 088$ (magenta) and $f = 0.51$ (blue-green); bifurcation diagrams $y(\Omega)$: $f = 0.037$ (magenta) and $f = 0.51$ (blue-green).

5.2 Large orbits: singular points, jumps, and escape phenomena

The Type II singular points can be computed from the expressions listed in Table 1.

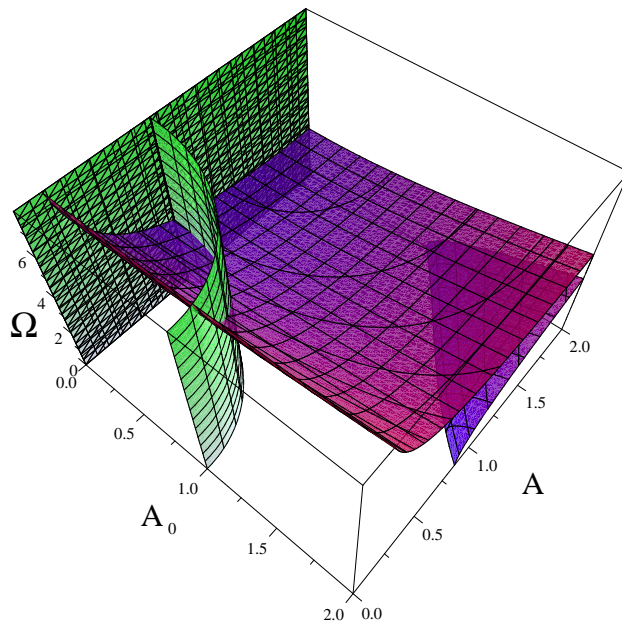


Figure 5: Intersection of surfaces: $K_1(A_0, A) = 0$ (green) and $K_2(A_0, A, \Omega) = 0$ (blue and red), $h = 0.5$, $c = 0.5$, $f = 10$.

The surfaces $K_1(A_0, A) = 0$ (green) and $K_2(A_0, A, \Omega) = 0$ (blue and red) are shown in Fig.5 for $h = 0.5, c = 0.5, f = 10$. For these parameter values, we compute, from the formulas listed in Table 1, $\Omega = 2.836, A = 1.155$. Therefore, the intersection point of green (two patches) and blue and red surfaces has the coordinates $(A_0, A, \Omega) = (0, 1.155, 2.836)$ in Fig.5 and $(A, \Omega) = (1.155, 2.836)$ in Fig.6, see the red dot denoted as "1". The black dashed line denotes the borderline solution of Table 2.

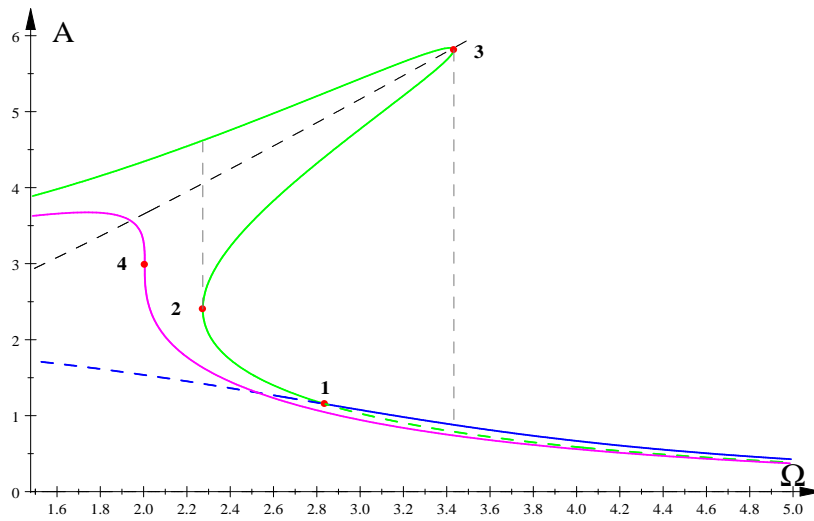


Figure 6: Implicit functions: $L_1(A, \Omega; 0.5, 0.5, 10) = 0$ (blue), $L_2(A, \Omega; 0.5, 0.5, 10) = 0$ (green), $L_2(A, \Omega; 1.446, 0.5, 10) = 0$ (magenta), and $L_2(A, \Omega; 0, 0.5, 0) = 0$ (black, dashed).

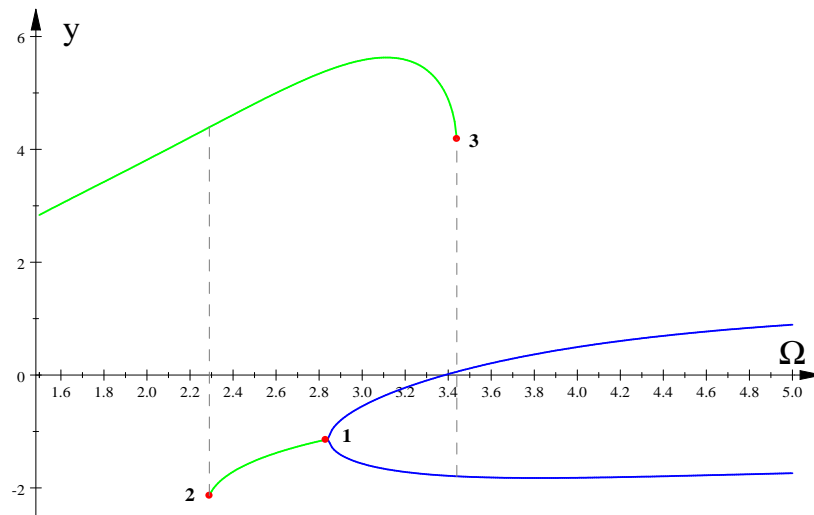


Figure 7: Bifurcation diagram $y(\Omega), h = 0.5, c = 0.5, f = 10$.

The bifurcation diagram computed for Eq.(3) is shown in Fig.7. The transition be-

tween small and large orbits occurs indeed near the critical value $\Omega = 2.836$.

Moreover, we have used equations (10) and (16) to study jump phenomena. The computed points of jumps (at vertical tangencies) and the corresponding points present in the bifurcation diagram are denoted in Figs.6 and 7 as "2" and "3".

We have also determined the onset of bistability for large orbits. In Figure 8 below, we show the implicit functions $L_2(A, \Omega; 1.446, 0.5, 10) = 0$ (the onset of bistability, magenta), $L_2(A, \Omega; 1.20, 0.5, 10) = 0$ (blue-green), as well as the bifurcation diagrams computed for Eq.(3), the same color lines correspond to the same states.

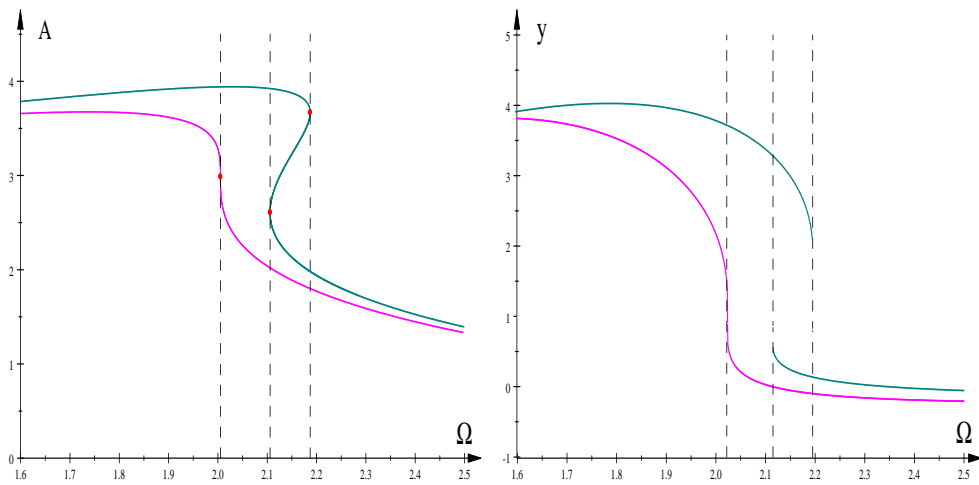


Figure 8: Functions $L_2(A, \Omega) = 0$: $c = 0.5$, $f = 10$, $h = 1.446$ (magenta), and $h = 1.20$ (blue-green); bifurcation diagrams $y(\Omega)$: $h = 1.43$ (magenta) and $h = 1.20$ (blue-green).

We can now describe a sequence of events, predicted by the form of the implicit functions $L_1 = 0$, $L_2 = 0$, cf. Fig.6, and confirmed by the bifurcation diagram, Fig.7, computed from Eq.(3).

Let $h = 0.5$, $c = 0.5$, $f = 10$, and $\Omega = 4.0$. In this case, the dynamics settles on either of two small orbits (blue), see Figs.6, 7. Then, for the decreasing values of Ω , the small orbit transforms into a large orbit of small amplitude (green) at point "1" (singular point). This large orbit, upon further decreasing of Ω , jumps at point "2" (vertical tangency point) to the large orbit with large amplitude (green). If the value of Ω is increased now, another vector tangency point ("3") is reached and the large orbit with large amplitude falls onto either of the small orbits (blue).

6 Conclusion

In this work, we have investigated several bifurcations present in the twin-well Duffing equation (1). We based our approach on the known steady-state asymptotic solution of the nondimensional Duffing equation (3) computed in implicit form, see Eqs.(4), (5a), (5b), and (6), (7).

Working in the framework of the differential properties of implicit functions [11–13], we have computed (i) singular points in the 3D formulation and (ii) 2D singular points in

Sections 3, 4, (iii) the points of vertical tangencies, and (iv) the double points of vertical tangencies in Section 4.

Case (i) corresponds to the small orbit – large orbit transition (escape phenomenon), see point "1" in Figs.6, 7. Case (ii) is a rupture of a stable branch of a small orbit solution, see Figs.2, 3, while case (iii) corresponds to jumps, see for example points "2", and "3" in Figs.6, 7. Finally, case (iv) coincides with the onset of bistability, after which jumps are possible, see Fig.4 and Figs.6, 8.

Our analytical predictions correlate well with the numerical computations carried out for the Duffing equation (3) and are reported in Section 5, the agreement is very good in the case of the large orbit and satisfactory for the small orbit (this shows that the large orbit asymptotic solution 7 is definitely more exact than the small orbit one 6).

References

- [1] W. Szemplińska-Stupnicka. *Chaos, Bifurcations and Fractals Around Us: A Brief Introduction*. Vol. 47. World Scientific, 2003.
- [2] S. Lenci and G. Rega. Forced harmonic vibration in a Duffing oscillator with negative linear stiffness and linear viscous damping. In: *The Duffing Equation: Nonlinear Oscillators and Their Behavior* (Eds.: I. Kovacic, M.J. Brennan). John Wiley & Sons, Hoboken, New Jersey, 2011, 277–322.
- [3] P.J. Holmes. A Nonlinear Oscillator with a Strange Attractor. *Phil. Trans. R. Soc. Lond. A* **292** (1979) 419–448.
- [4] F.C. Moon and P.J. Holmes. A Magnetoelastic Strange Attractor. *Journal of Sound and Vibration* **65** (1979) 275–296.
- [5] I. Kovacic and M.J. Brennan, Eds. *The Duffing Equation: Nonlinear Oscillators and Their Behavior*. John Wiley & Sons, Hoboken, New Jersey, 2011.
- [6] J. Kyzioł and A. Okniński. Asymmetric Duffing Oscillator: Jump Manifold and Border Set. *Nonlinear Dyn. Syst. Theory* **23** (2023) 46–57.
- [7] J. Awrejcewicz, Modified Poincaré method and implicit function theory. In: *Nonlinear Dynamics: New Theoretical and Applied Results* (Ed.: J. Awrejcewicz). Akademie Verlag, Berlin, 1995, 215–229.
- [8] Nayfeh, A.H. *Introduction to Perturbation Techniques*. John Wiley & Sons, 2011.
- [9] M. Wali Ullah, M. Alhaz Uddin and M. Saifur Rahman. A Modified Harmonic Balance Method for Solving Strongly Generalized Nonlinear Damped Forced Vibration Systems. *Nonlinear Dyn. Syst. Theory* **21** (2021) 544–552.
- [10] D.W. Jordan and P. Smith. *Nonlinear ordinary differential equations*. Oxford University Press Inc., New York, Fourth edition, 2007.
- [11] G.M. Fikhtengol'ts, (I.N. Sneddon, Ed.). *The fundamentals of mathematical analysis*. Vol. 2, Elsevier, 2014 (Chapter 19).
- [12] E. Hartmann. *Geometry and Algorithms for Computer-Aided Design*. Darmstadt University of Technology, Darmstadt, 2003.
- [13] C.T.C. Wall. *Singular Points of Plane Curves*. Cambridge University Press, New York, 2004.
- [14] P.J. Holmes and D.A. Rand. The bifurcations of Duffing's equation: an application of Catastrophe Theory. *J. Sound Vib.* **44** (1976) 237–253.
- [15] T. Kalmár-Nagy and B. Balachandran. Forced harmonic vibration of a Duffing oscillator with linear viscous damping. In: *The Duffing Equation: Nonlinear Oscillators and Their Behavior* (Eds.: I. Kovacic, M.J. Brennan). John Wiley & Sons, 2011, 139–174.

- [16] A.K. Mallik. Forced harmonic vibration of a Duffing oscillator with different damping mechanisms. In: *The Duffing Equation: Nonlinear Oscillators and Their Behavior* (Eds.: I. Kovacic, M.J. Brennan). John Wiley & Sons, Hoboken, New Jersey 2011, 175–217.
- [17] J. Kyzioł. Metamorphoses of resonance curves for two coupled oscillators: The case of small non-linearities in the main mass frame. *Int. J. Nonlinear Mech.* **76** (2015) 164–168.
- [18] W. Szemplinska-Stupnicka. Bifurcations of harmonic solution leading to chaotic motion in the softening type Duffing's oscillator. *Int. J. Nonlinear Mech.* **23** (1988) 257–277.
- [19] M.P. Markakis. The jump phenomenon associated with the dynamics of the duffing equation. *Physics Open* **5** (2020) 100042.
- [20] S. Janson. Resultant and discriminant of polynomials. Lecture notes, 2010. Available at <http://www2.math.uu.se/~svante/papers/sjn5.pdf>